The Dynamics of Groundwater Flow and Salinity Transport in Unconfined Coastal Aquifers(Supplement)

AUTHOR(S):

Kriyo, Sambodho

The Dynamics of Groundwater Flow and Salinity Transport in Unconfined Coastal Aquifers

View of the Taniyagi Beach, a study site selected

Kriyo Sambodho

2009

Physical processes operating in beach system

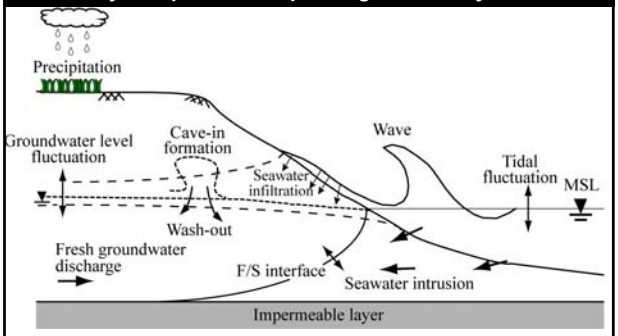

Fig. 1.1

Coastal aquifer undergo complex and dynamic hydro-geological processes

INTRODUCTION

Organization of the thesis

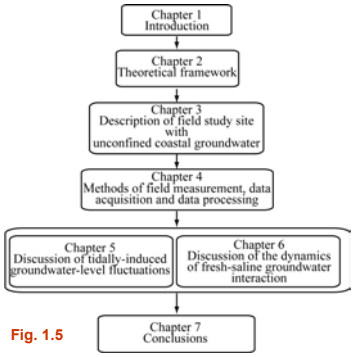

Fig. 1.5

The 2001 Okura Beach tragedy

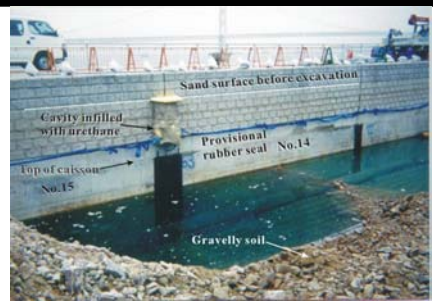

View of cavity formation in Okura Beach (Sekiguchi et al., 2002)

The Okura Beach tragedy calls for a thorough study of the geo-hydrodynamical performances of **nourished sandy beaches**.

Purposes

Deeper understanding :

1. Groundwater table variations due to diurnal and semidiurnal tidal changes.
2. Long-term variations of groundwater table in unconfined aquifer.
3. Unsteady groundwater responses to extreme events such as typhoon-induced storm surges.
4. Development of freshwater zone in nourished sandy beaches.
5. The dynamics of fresh-saline groundwater interactions.

Outcome:
Deeper understanding of the coastal groundwater environments that include the performance of shallow-penetrated coastal wells in low-laying coastal area where freshwater are invaluable resources for potable water or for agricultural purposes.

THEORETICAL FRAMEWORK

1D analysis of tidally induced groundwater level fluctuation

$$\frac{\partial \eta}{\partial t} = C\frac{\partial^2 \eta}{\partial x^2}$$

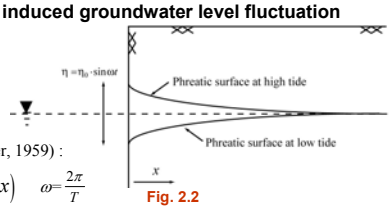

Solution (Carslaw&Jaeger, 1959) :

$$\eta = \eta_0 \cdot e^{-\lambda x}\sin\left(\omega t - \lambda x\right) \qquad \omega = \frac{2\pi}{T}$$

Fig. 2.2

$$\lambda = \left[\frac{\omega}{2C}\right]^{1/2}$$

The transfer coefficient C :

$$C = \frac{k\,d}{n} \quad \text{(Unconfined aquifer)}$$

$$C = \frac{k}{m_v \gamma_w} \quad \text{(Confined aquifer)}$$

Essential aspects: Amplitude decay and phase lag with increasing distance x from shoreline

Landward extent of wave- or tidally-induced groundwater level fluctuations

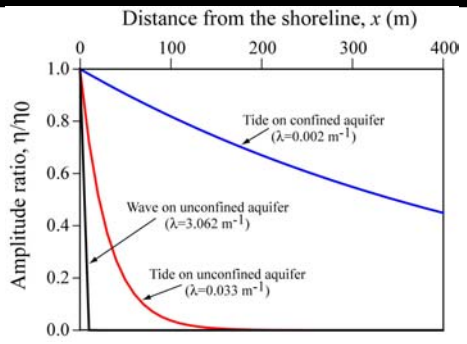

Fig. 5.23 Patterns of amplitude decay in wave- or tidally induced groundwater level fluctuations in unconfined or confined aquifers.

Solution procedures for saturated/ unsaturated groundwater flows

The three sets of primary unknowns:

- Displacement increments $\Delta U(J)$
- Pore air pressures u_a (J)
- Pore water pressures u_w (J).

$$\sigma''_{ij} = \sigma_{ij} - u_a \delta_{ij}$$

$$s = u_a - u_w$$

Solving Eqs. I and II $\rightarrow$ $\begin{bmatrix} K_1 & K_2 \\ K_3 & K_4 \end{bmatrix} \begin{Bmatrix} \Delta U \\ u_a \end{Bmatrix} = \begin{Bmatrix} f_1 \\ f_2 \end{Bmatrix}$

Solving Eq. III $\rightarrow$ $[K]\{u_w\} = \{R\}$

THEORETICAL FRAMEWORK

Two-dimensional analysis procedure for saturated/ unsaturated groundwater flows

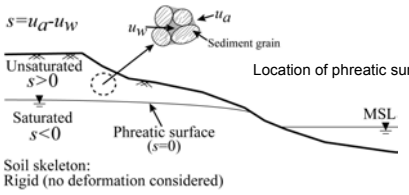

Location of phreatic surface is part of the solution

The incorporation of the unsaturated domain facilitates the estimation of phreatic surface location.

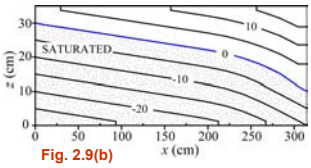

Fig. 2.9(b)

Validating of 2D groundwater flow model

VALIDATION

- Experimental results from Uno (1970)
- Dupuit-Forchheimer quasi-static solution

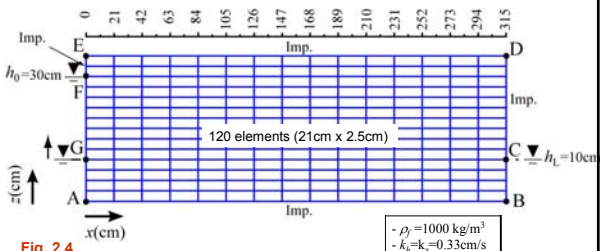

Fig. 2.4

F-A: $h_p = \gamma_w (h_0 - z)$

B-C: $h_p = \gamma_w (h_L - z)$

- ρ_f =1000 kg/m^3
- k_h=k_x=0.33cm/s
- n=0.44
- S_{rd}=0.085
- a=4 kPa
- b=2 kPa
- c= 0.9

Governing equations for saturated/ unsaturated groundwater flows

Equilibrium equations for saturated-unsaturated porous media

$$\frac{\partial \sigma''_{ji}}{\partial x_j} + \frac{\partial u_a}{\partial x_j}\delta_{ij} + b_i = 0 \qquad b_i: \text{ body force. } u_a: \text{pore air pressure} \qquad \text{I}$$

Mass conservation equations

Pore air :

$$\rho_a (1-S_w)\frac{\partial \varepsilon_v}{\partial t} - n(1-S_w)\frac{\partial \rho_a}{\partial t} + \rho_a n \frac{\partial S_w}{\partial t} = -\frac{\partial}{\partial x}\left(\rho_a \frac{k_a}{\gamma_w}\frac{\partial u_a}{\partial x}\right) - \frac{\partial}{\partial z}\left(\rho_a \frac{k_a}{\gamma_w}\frac{\partial u_a}{\partial z}\right) \qquad \text{II}$$

$$\frac{\partial \rho_a}{\partial t} = \frac{\rho_a}{u_a + p_{at}}\frac{\partial u_a}{\partial t}$$

Pore water:

$$S_w \frac{\partial \varepsilon_v}{\partial t} - n C_s \frac{\partial s}{\partial t} = -\frac{\partial}{\partial x}\left(\frac{k_w}{\gamma_w}\frac{\partial u_w}{\partial x}\right) - \frac{\partial}{\partial z}\left(\frac{k_w}{\gamma_w}\frac{\partial u_w}{\partial z} + k_w\right) \qquad \text{III}$$

Development of phreatic surface

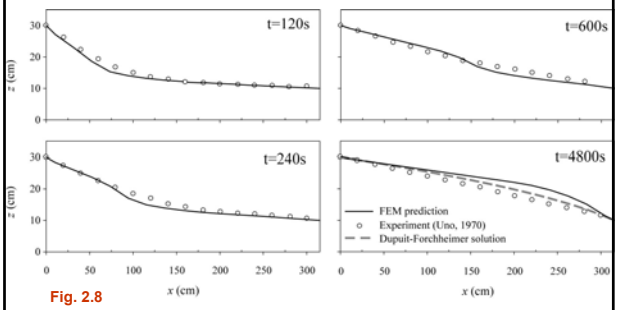

Fig. 2.8

The present FE analysis is in reasonable agreement with the experimental performance by **Uno** (1970) and with the Dupuit-Forchheimer quasi-static solution.

Sharp-interface approach using Ghyben-Herzberg assumption

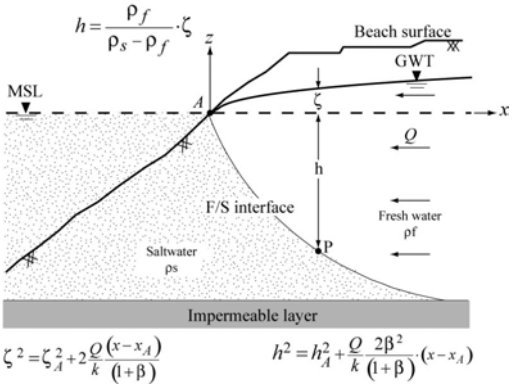

$$h = \frac{\rho_f}{\rho_s - \rho_f} \cdot \zeta$$

$$\zeta^2 = \zeta_A^2 + 2\frac{Q}{k}\frac{(x - x_A)}{(1+\beta)} \qquad h^2 = h_A^2 + \frac{Q}{k}\frac{2\beta^2}{(1+\beta)} \cdot (x - x_A)$$

THE FIELD STUDY SITE SELECTED

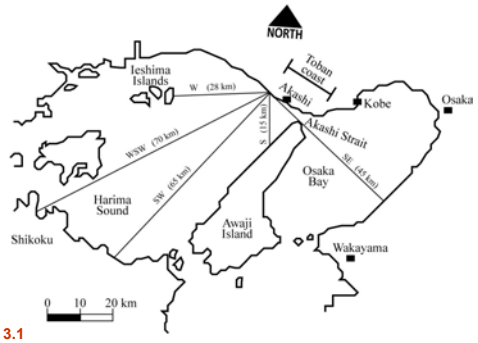

Fig. 3.1

Location map of Toban coast facing Harima Sound (Kadomatsu et al., 1991)

Glover solution for freshwater-seawater interactions

The aquifer is homogeneous, confined at the top and unbounded at the bottom.

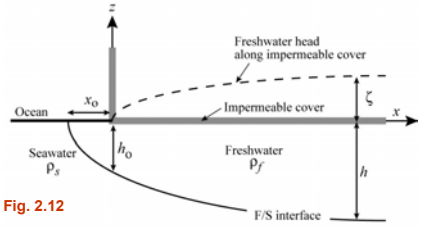

Fig. 2.12

$$\zeta_{z=0} = \sqrt{\frac{2Q}{\beta k}x} \qquad h = \sqrt{2\beta\frac{Q}{k}x + \left(\frac{Q}{k}\right)^2\beta^2} \qquad x_0 = \frac{\beta}{2}\frac{Q}{k} \qquad h_0 = \beta\frac{Q}{k}$$

(Glover, 1964)

The outflow face terminates at a certain depth under the sea

Erosion history of Toban coast

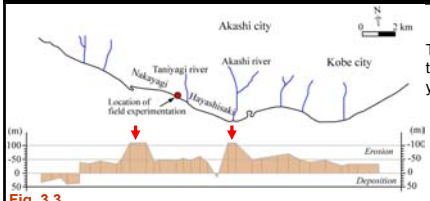

Fig. 3.3

The extent of erosion on the Toban coast during years 1893-1955

Fig. 3.4

(a) Situation in Matsue area and (b) Situation in Eigashima area in 1964

Sea cliff + gently platform → Very vulnerable to coastal erosion.

Advection-dispersion equations for density-dependent flow

Darcy's law for density-dependent groundwater flow

$$u_x = -k_x\frac{\partial}{\partial x}\left(\frac{P}{\rho_f g}\right); \quad u_z = -k_z\left(\frac{\partial}{\partial z}\left(\frac{P}{\rho_f g}\right) + \frac{\rho}{\rho_f}\right)$$

Mass conservation for density-dependent groundwater flow

$$S_w\frac{\partial \varepsilon_v}{\partial t} - nC_s\frac{\partial s}{\partial t} + \beta S_w n\frac{\partial s}{\partial t} = -\frac{1}{\rho}\frac{\partial}{\partial x}\left(\rho k_x\frac{\partial}{\partial x}\left(\frac{P}{\rho_f g}\right)\right) - \frac{1}{\rho}\frac{\partial}{\partial z}\left(\rho k_z\left(\frac{\partial}{\partial z}\left(\frac{P}{\rho_f g}\right) + \frac{\rho}{\rho_f}\right)\right)$$

Relation between salinity and density

$$\frac{\rho - \rho_f}{\rho_f} = C\cdot\left(\frac{\rho_s - \rho_f}{\rho_f}\right)$$

Mass conservation for saline transport

$$\frac{\partial \theta C}{\partial t} + \underbrace{\frac{\partial (u_x C)}{\partial x} + \frac{\partial (u_z C)}{\partial z}}_{\text{Advection}} = \underbrace{\frac{\partial}{\partial x}\left(\theta D_{xx}\frac{\partial C}{\partial x}\right) + \frac{\partial}{\partial z}\left(\theta D_{zz}\frac{\partial C}{\partial z}\right)}_{\text{Diffusion}}$$

Erosion history of Toban coast

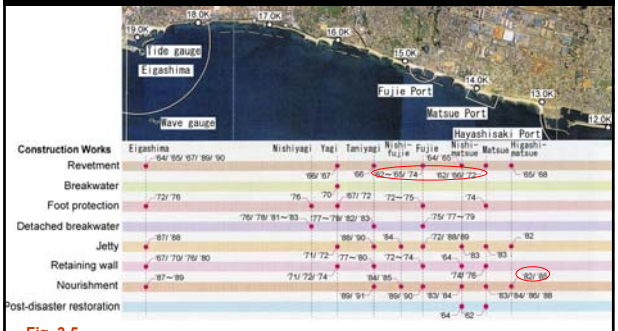

Fig. 3.5

Stages of shore protection work on Toban coast (Himeji office, MLIT, 2003)

Extensive beach nourishment project has been performed since 1982

THE FIELD STUDY SITE SELECTED

Taniyagi Beach in Toban coast

Study area: Nourished sandy beach with gently slopping shore platform and extends in front of the sea cliff of Pleistocene soil

Fig. 3.6

FIELD MEASUREMENTS AND DATA ACQUISITION METHODS

Field measurements

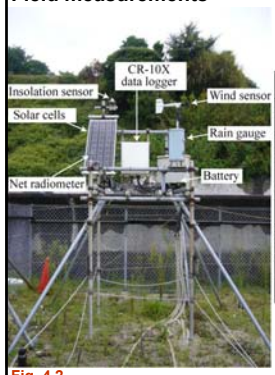

Meteorological	Geo-hydrological
1. Air temperature	1. Soil suction
2. Humidity	2. Soil moisture
3. Rainfall intensity	3. Groundwater level
4. Wind direction and wind velocity	4. Groundwater salinity
5. Atmospheric pressure	5. Groundwater temperature
6. Solar radiation	6. Soil temperature
7. Radiation balance	7. Tide level at nearby Fujie port

(Azuma et al., 2005)

Fig. 4.2

Geological settings

Cross-shore profile of the study area with representative boring logs and SPT test results

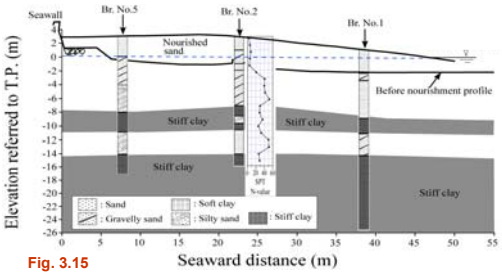

Fig. 3.15

1. Well-defined unconfined aquifer above stiff clay layer
2. The unconfined aquifer includes of the nourished sand layer about 3m thick.

Tide level measurement

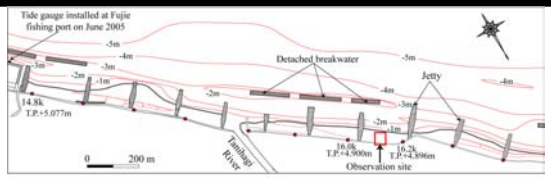

Fig. 4.1

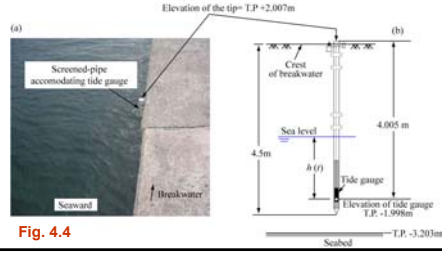

Fig. 4.4

Geological settings

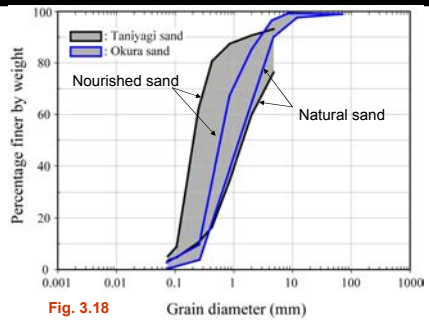

Fig. 3.18

Grain-size distributions of the samples taken from Br. No 2 at Taniyagi Beach compare with the Okura sand

Groundwater level measurement

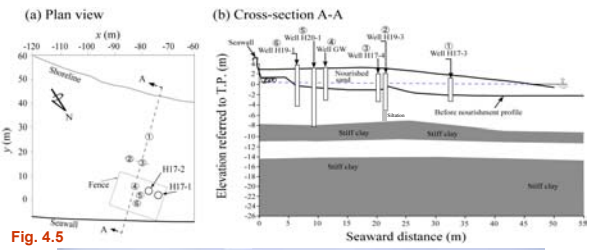

Fig. 4.5

Fig. 4.6

Suction measurement

Soil suction $s = u_a - u_w$

A total of six electric tensiometers (UNSUCs) were installed at soil depths of 0.2m, 0.5m, 0.8m, 1.2m, 1.6m and 2.0m from the sand surface

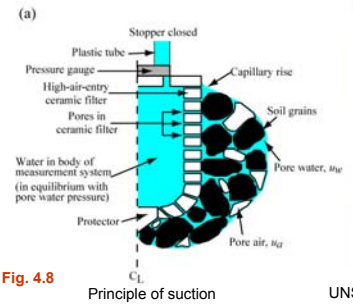

Fig. 4.8

Principle of suction measurement

UNSUC for single-level measurement

Salinity measurement

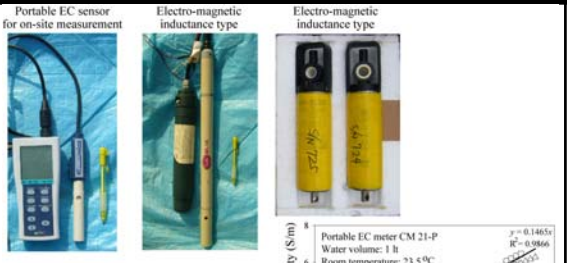

Fig. 4.10

Electro-magnetic inductance type EC sensors:
-No direct contact with saltwater needed.
-Built-in data logger.
→ Permitting continuous EC measurements.

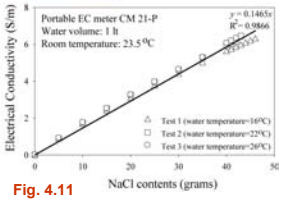

Fig. 4.11

Data acquisition methods

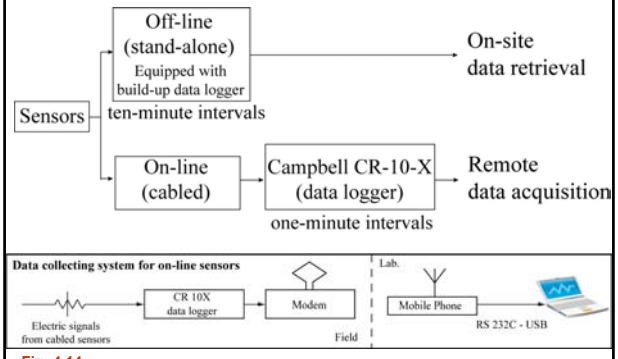

Fig. 4.14

TIDALLY INDUCED GROUNDWATER FLUCTUATIONS

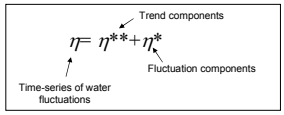

1. Moving average method

To resolve the trend components (seasonal effects) of the time-series data.

2. Fourier transform technique

To resolve the fluctuation components of de-trended time-series data.

Important observations:
1. Correspondence between tidal and groundwater fluctuations.
2. Amplitudes decreasing with increasing distance x from the shoreline.

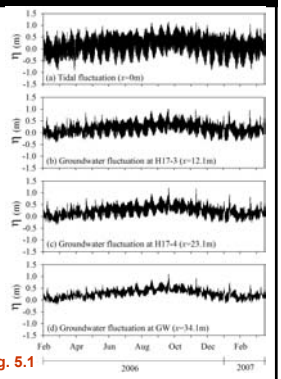

Fig. 5.1

Evolution of water-level fluctuations over a representative one-year period on Taniyagi Beach

Trend components of tides and groundwater fluctuations

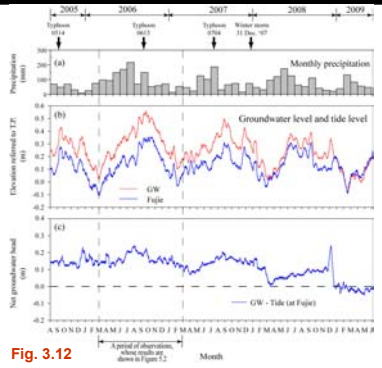

Fig. 3.12

The net groundwater head was positive in the first three years, implying fresh groundwater discharge to the sea.

Trend components of tides and groundwater fluctuations

Findings:

1. The tide level is highest in summer and is lowest in winter →Seasonal variation

2. The slow groundwater-level variations are in phase with evolution of tide level

3. The inland groundwater levels are well above the tide level → Freshwater discharge

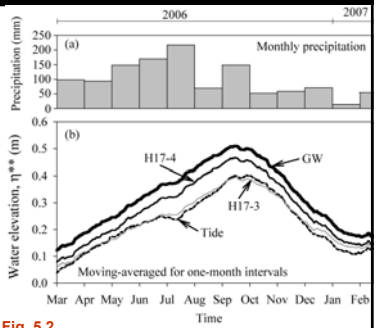

Fig. 5.2

(a) monthly precipitation and (b) the trend components of the tide and groundwater-level fluctuations at the three wells (GW, H17-4 and H17-3) on Taniyagi Beach

Harmonic components of tidal fluctuations

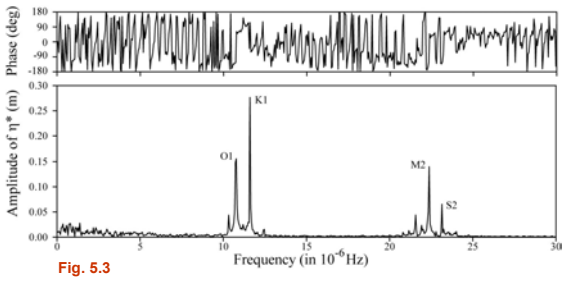

Fig. 5.3

Dominant tidal components:

- K_1 : Luni-solar declination diurnal (T=23.9h)
- O_1: Lunar declination diurnal (T=25.8h)
- M_2: Principal lunar semidiurnal (T=12.4h)
- S_2: Solar declination semidiurnal (T=12.0h)

Characteristics of tidally-induced groundwater responses

The transfer coefficient of aquifer C can be determined from a full-scale "field experiment" using the tidal response technique.

	Diurnal component	Semi-diurnal component
λ	0.032 m^{-1}	0.048 m^{-1}
C	0.0356 m^2/s	0.0332 m^2/s
C_{AVG}	**0.0335 m^2/s**	

Tidal response technique is effective and reliable for estimating aquifer parameters in the coastal region.

Harmonic components of tidal fluctuations

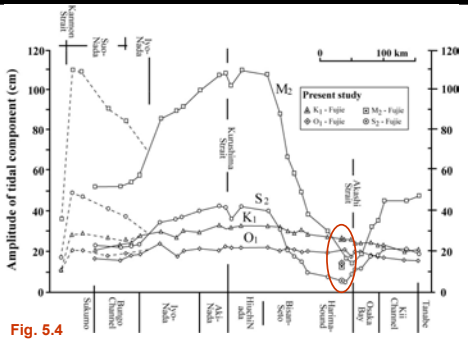

Fig. 5.4

Amplitudes of dominant tidal components at **Fujie port** (Present Study) are compatible with the field performance in the Seto Inland Sea reported by Fujiwara (1981).

Event-accentuated groundwater-level response

The field performances

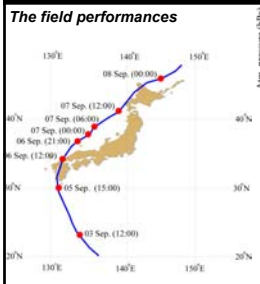

Fig. 5.7

Track of typhoon 0514 (Digital Typhoon, 2005)

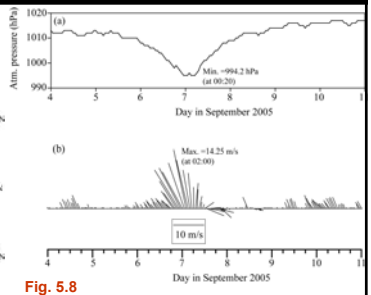

Fig. 5.8

(a)Time histories of atmospheric pressure and (b) Hourly wind vectors, both were recorded on Taniyagi Beach

Characteristics of tidally-induced groundwater responses

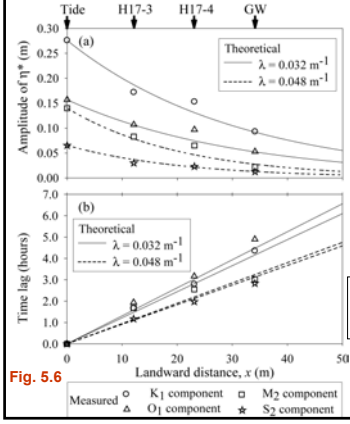

Fig. 5.6

$$\eta^* = \eta_0^* \cdot e^{-\lambda x} \sin(\omega t - \lambda x)$$

$$\lambda = \left[\frac{\omega}{2C}\right]^{1/2} \quad \text{and} \quad C = \frac{k \cdot d}{n}$$

Amplitude decay and increasing time lag with increasing distance x from the shoreline.

Tidal variations and groundwater fluctuations at well GW

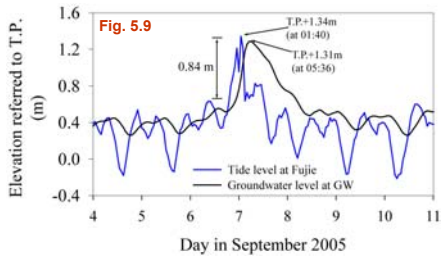

Fig. 5.9

- The tide peaked at 01:40 on 7 September 2005, exhibiting a storm surge of 0.84m.
- The groundwater fluctuations in well GW peaked at 05:36, with 4-hour lag in response.
- The rise of groundwater-level at GW (=0.88m) was very close to the storm surge.

Groundwater level responses to a storm surge

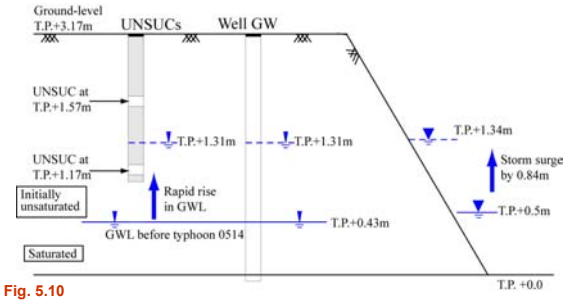

Fig. 5.10

Evidences that captures the event-accentuated groundwater level response.

Storm surge effect on groundwater-level fluctuations: 2D FE Analysis

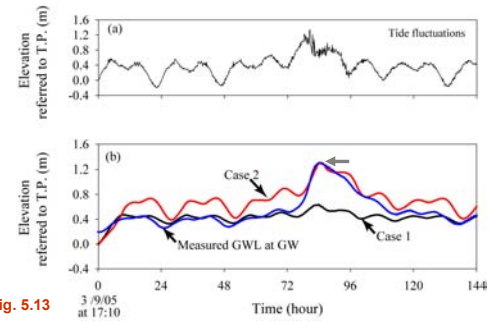

Fig. 5.13

Case 2 (with impermeable landward boundary) is close to the measured performance of storm-surge induced rapid rise in groundwater-level at well GW

Performance of suction measurements

Effects of precipitation only visible at shallow depths

The UNSUC -2.0m (T.P.+1.17m) recorded a negative suction (equivalent to a positive water-pressure head 0.14m) → Submergence of the UNSUC

Groundwater level measured by UNSUC -2.0m
→1.17m + 0.14m =1.31m

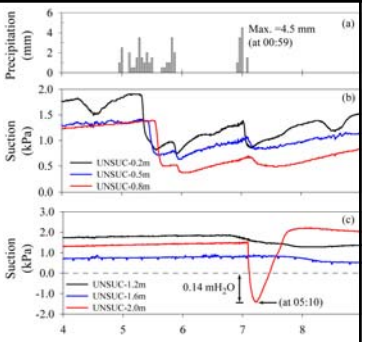

Fig. 5.11

The event-accentuated rise in the groundwater level was independently supported by suction measurement at T.P.+1.17m

Storm surge effect on groundwater-level fluctuations: 2D FE Analysis

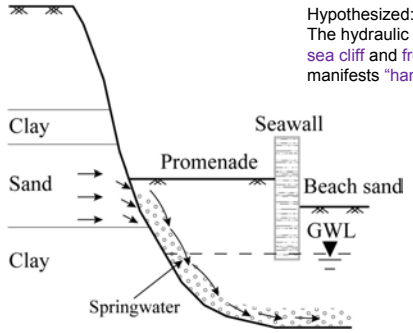

Hypothesized:
The hydraulic linkage between sea cliff and frontal sand beach manifests "hanging springwater"

When the seawater level becomes considerably high, the face of the sea cliff will act as an essentially impermeable boundary

Storm surge effect on groundwater-level fluctuations: 2D FE Analysis

Finite element mesh and parameters

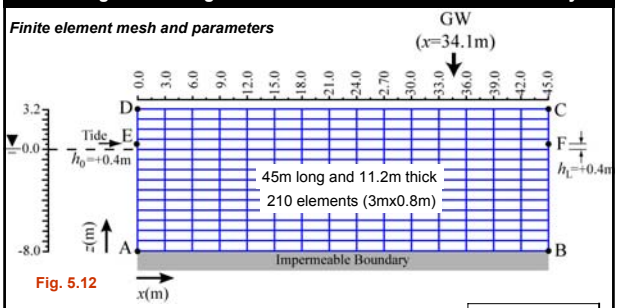

Fig. 5.12

	Case I	Case II
Boundary conditions	-Bottom: impermeable **-Landward: permeable** -Top: impermeable -Seaward: Permeable	-Bottom: impermeable **-Landward: impermeable** -Top: impermeable -Seaward: permeable

- ρ_f=1000 kg/m^3
- k_h=k_z=0.002m/s
- e=0.67
- n=0.4
- P_c=4.0 kPa
- a=0.35 kPa^{-1}
- b=3.5 kPa

DYNAMICS OF FRESH-SALINE GROUNDWATER INTERACTION

Tide effects on tempo-spatial structure of aquifer salinity

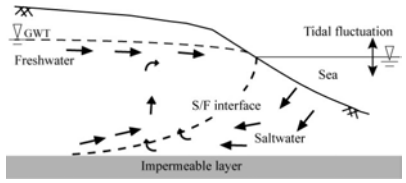

Investigating the extent of saltwater intrusion at various depths as influenced by tidal fluctuations.
→ Deeper understanding of groundwater-seawater flow interactions which may include seawater circulation.

Approach:
High-resolution field measurements of groundwater salinity changes and groundwater fluctuations in the observation wells together with tidal variations.

Tide effects on tempo-spatial structure of aquifer salinity

Performance of continuous EC measurements in two observation wells

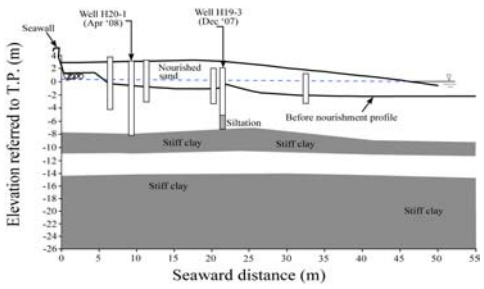

Groundwater EC at the two wells was measured using two EC sensors of electromagnetic-inductance type

Performance of continuous EC measurements in two obs. wells

Measurements at T.P.-5.5m **Fig. 6.7(4)**

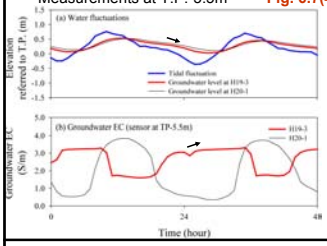

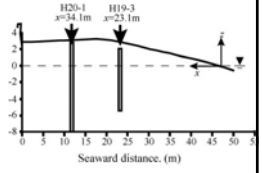

H19-3 (x=23.1m) at **FALLING TIDE**

$$\frac{\partial C}{\partial t} = -u_x \frac{\partial C}{\partial x} - u_z \frac{\partial C}{\partial z}$$

1. Seaward groundwater flow: $u_x < 0$
2. EC at H19-3 > EC at H20-1 $\frac{\partial C}{\partial x} < 0$

$$-u_x \frac{\partial C}{\partial x} < 0$$

3. EC at H19-3 increases with time: $\frac{\partial C}{\partial t} > 0$

So $u_z \frac{\partial C}{\partial x} < 0$

4. EC increases with depth: $\frac{\partial C}{\partial z} < 0$

$u_z > 0$

UPWARD GROUNDWATER FLOW IMPORTANT

Performance of continuous EC measurements in two obs. wells

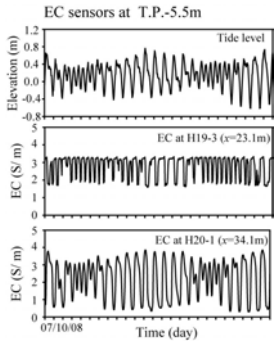

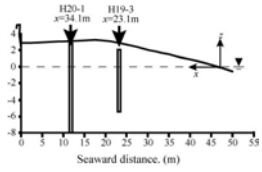

Fig. 6.3

Main findings:

- Strong correlation between EC variations and tidal fluctuations.
- Constant peaks and troughs at x=23.1m indicate mixing of fresh groundwater & seawater.

Performance of continuous EC measurements in two obs. wells

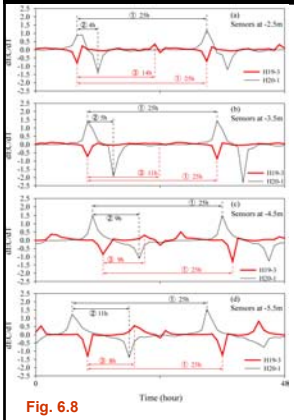

Fig. 6.8

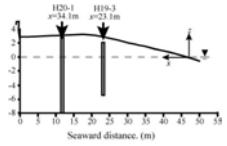

Main findings

①: Time difference between the two highest peaks (or two lowest troughs) → Period of diurnal fluctuation

②: Effect of seawater intrusion → Deeper location, longer effect

③: Time response of circulated seawater (only appear at H19-3) → Deeper location, faster response

Performance of continuous EC measurements in two obs. wells

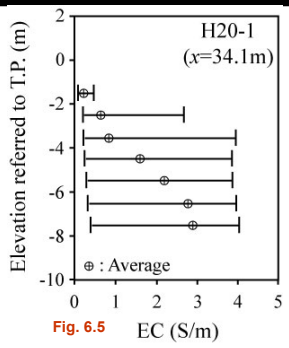

Fig. 6.5

Main findings:

1. Fresh groundwater body at above T.P.-2m or so at x=34.1m.
2. Low EC values at low tide suggesting the accentuated fresh groundwater discharge to the sea.

Performance of intensive EC measurements in cross-shore array

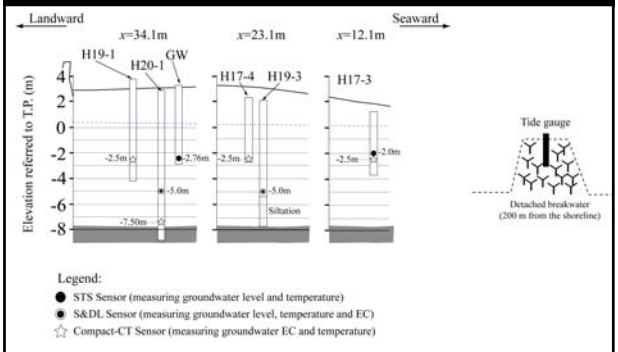

Fig. 6.9

Layout of instruments used during intensive field measurements (18 May – 3 June 2009).

Performance of intensive EC measurements in cross-shore array

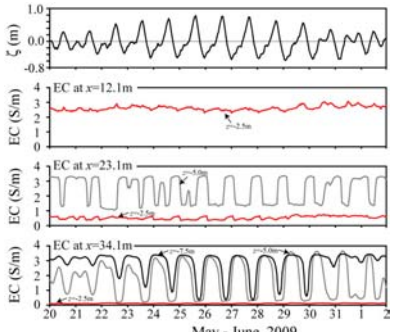

Fig. 6.11

Findings:
1. Availability of fresh groundwater body at shallow depth at x=23.1m and x=34.1m.
2. EC values dynamically change with tide at deeper depths.

Fresh-saline groundwater interaction

High Tide : Maximum saltwater penetration. Saltwater pushes the freshwater further inland. Heavier saltwater move underneath the lighter freshwater.
Falling Tide : Fresh groundwater flows seaward. Upward seawater flow at x=23.1m.
Low Tide : Minimum seawater intrusion. Fresh groundwater discharges at maximum.
Rising Tide : Saltwater starts to intrude and reaches maximum state at following high tide.

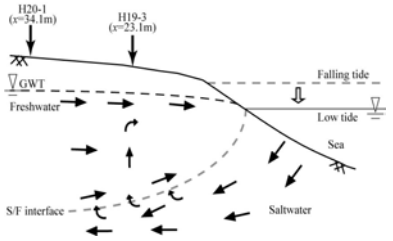

Fig. 6.14

Performance of intensive EC measurements in cross-shore array

Average values of groundwater EC in cross-shore array at three depths of measurement.

EC seawater=4.61S/m

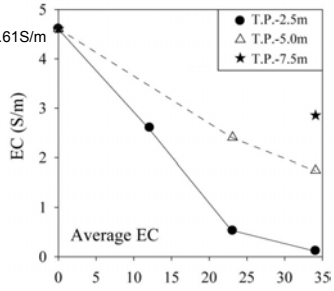

Fig. 6.12

EC systematically decreases with increasing distance landwards

Performance of fresh groundwater discharge into sea

Observed long-term performance of precipitation and water level fluctuations

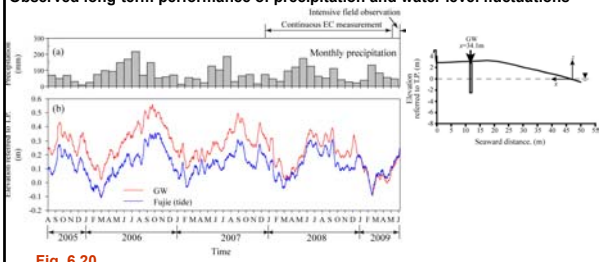

Fig. 6.20

Important observations:
1. Groundwater fluctuations consistently follow the pattern of tidal fluctuations.
2. The tidal and groundwater levels are high in summers and low in winters.
3. Tide levels are higher than groundwater levels in the first five months in year 2009.

Stages of maximum and minimum seawater intrusion

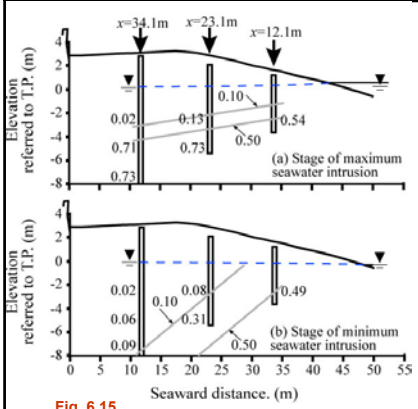

Fig. 6.15

Findings:

- Depth to the F/S interface decreases as the shoreline is approached.
- Thickness of the diffusion zone = 1.2m.
3. Freshwater pushes salt water to the sea.
4. Thicker diffusion zone.

Net groundwater head and normalized fresh groundwater discharge

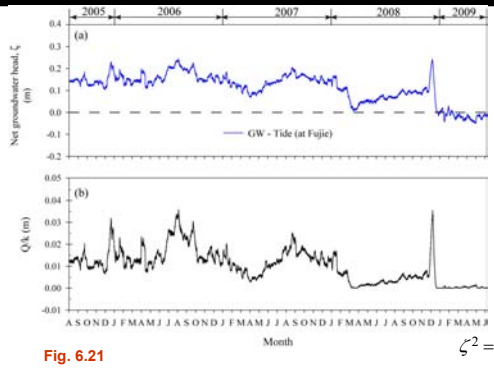

Fig. 6.21

$$\zeta^2 = 2\frac{Q}{k}\frac{x}{(1+\beta)}$$

Fresh groundwater discharge amounts to Q/k=0.01m on average for the first three years.

Assessment of fresh groundwater discharge Q to the sea

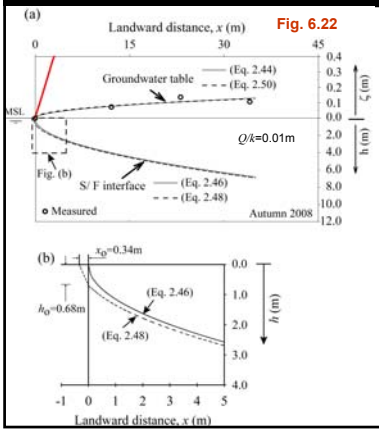

Obtained using tidal response technique
C=0.0335m²/s

$$Q = \frac{Q}{k} \cdot \frac{C \cdot n}{d}$$

=1.45m³/day per running meter

(n=0.4; d=8m)

Seasonal evolution of freshwater-saline water interface

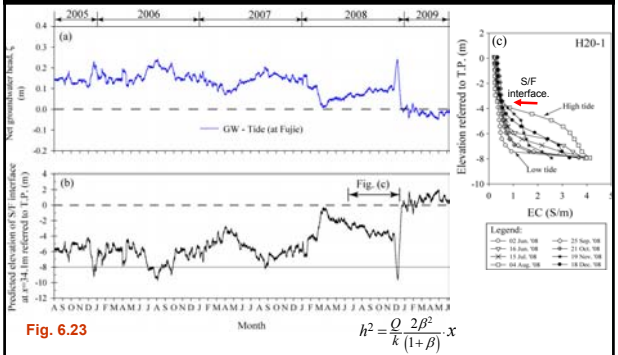

Fig. 6.23

$$h^2 = \frac{Q}{k} \frac{2\beta^2}{(1+\beta)} \cdot x$$

The predicted depth h to S/F from June-December 2008 approximates to the observed depth 4.2m from EC measurements

What happened when the net groundwater head ζ was negative in value ?

Observed performance during the early five months in year 2009

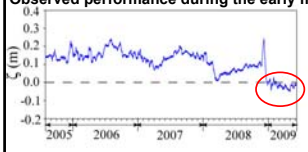

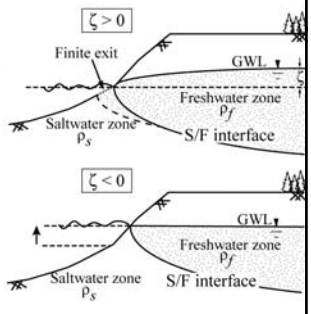

Hypothesis for persistency of freshwater body:

When $\zeta > 0$ → The exit remains open.

When $\zeta < 0$ → The width of the outlet reduces to zero, eventually permitting the freshwater body to sustain.

CONCLUSIONS

Tidally induced groundwater fluctuations

1. The measured performances of the tide and groundwater level fluctuations in the three observation wells on a cross-shore array over a representative one-year period show the consistent positive correlations between them.
2. The trend components of tide and groundwater level fluctuations can be resolved by taking a moving average over the time-series data. The identified trend components indicate that the inland groundwater heads are systematically higher than the tidal level, revealing the occurrence of fresh groundwater discharge toward the sea.
3. The Fourier spectral analyses of the de-trended tidal data permitted the identification of the four dominant harmonic components, K_1, O_1, M_2 and S_2. The amplitudes of the dominant tidal components at Fujie port are compatible with the field performance in the Seto Inland Sea reported by Fujiwara (1981).
4. The application of Fourier analyses facilitated the evaluation of the amplitude decay and time lag of groundwater responses to each of the dominant tidal components, in a manner compatible with the theoretical predictions. The tidal-response procedure thus proves to be a reliable one, facilitating the identification of the aquifer transfer coefficient (C) under field conditions.

CONCLUSIONS (Contd.)

5. The continuous measurements of tide and groundwater level variations captured the event-accentuated groundwater responses during typhoon-induced storm surge on 6 September 2005. The storm surge induced a rapid rise of the groundwater table by 0.88m. The event-accentuated rise in the groundwater level was independently supported by the sharp drop in the soil suction measurement at elevation T.P.+1.17m.
6. The groundwater fluctuations predicted using 2D FE analyses reproduce nicely the measured performance of groundwater fluctuations during the passage of typhoon 0514 and suggests that the hydraulic linkage between the sea cliff and frontal sand beach manifests “hanging springwater”.

Dynamics of fresh-saline groundwater

1. The availability of the fresh groundwater body in the unconfined aquifer concerned was confirmed from the measured performance of groundwater EC. The groundwater EC in well H20-1 at T.P.-1.5m is as low as 0.23 S/m and increases to 2.92 S/m at T.P.-7.5m, indicating that a body of fresh groundwater overlies more saline groundwater.
2. The occurrence of upward saline transfer during falling tide stage was evidenced, typically from the field performance of groundwater EC in well H19-3 (x=23.1m).

CONCLUSIONS (Contd.)

3. The dynamics of saltwater-freshwater interaction was captured in term of the intensive field measurements. At high tide the saltwater-freshwater interface moves landward and takes the stage of maximum seawater intrusion. In the following low tidal stage, the interface was pushed back to the sea by enhanced fresh groundwater flow. The thickness of the dispersion zone is found to be 1.2m at the stage of maximum seawater intrusion and it becomes wider at the stage of minimum seawater intrusion under low tide.
4. The long-term observations of groundwater conditions permitted the normalized fresh groundwater discharge (Q/k) to be determined at 0.01m on average.
5. The sharp-interface approach to estimating the configuration of saline water-freshwater interface is applicable to the situation when the net groundwater head inland is positive in value. This methodology, in combination with the tidal response method for determining the aquifer constant C, permitted an estimate of the fresh groundwater discharge to the sea on Taniyagi Beach; namely, Q=1.45 m³/ day per running meter of the beach.
6. The long-term field observations reveal that once a body of fresh groundwater is developed, it can withstand subsequent, continued exposures to tidal forcing as long as the hydrological conditions in the hinterland are maintained.